analytical chemistry

Article

pubs.acs.org/ac

MALDI MS In-Source Decay of Glycans Using a Glutathione-Capped Iron Oxide Nanoparticle Matrix

Qiaoli Liang,*[,†] Thomas Macher,[‡] Yaolin Xu,[‡] Yuping Bao,[‡] and Carolyn J. Cassady[†]

[†]Department of Chemistry, The University of Alabama, Tuscaloosa, Alabama 35487, United States

[‡]Department of Chemical and Biological Engineering, The University of Alabama, Tuscaloosa, Alabama 35487, United States

Supporting Information

ABSTRACT: A new matrix-assisted laser desorption ionization (MALDI) mass spectrometry matrix is proposed for molecular mass and structural determination of glycans. This matrix contains an iron oxide nanoparticle (NP) core with gluthathione (GSH) molecules covalently bound to the surface. As demonstrated for the monosaccharide glucose and several larger glycans, the mass spectra exhibit good analyte ion intensities and signal-to-noise ratios, as well as an exceptionally clean background in the low mass-to-charge (m/z) region. In addition, abundant in-source decay (ISD) occurs when the laser power is increased above the ionization threshold; this indicates that the matrix provides strong energy transfer to the sample. For five model glycans, ISD produced extensive glycosidic and cross-ring cleavages in the positive ion mode from singly charged precursor ions with bound sodium ions. Linear, branched, and cyclic glycans were employed, and all were found to undergo abundant fragmentation by ISD. ^{18}O labeling was used to clarify m/z assignment ambiguities and showed that the majority of the fragmentation originates from the nonreducing ends of the glycans. Studies with a peracetylated glycan indicated that abundant ISD fragmentation occurs even in the absence of hydroxyl groups. The ISD product ions generated using this new matrix should prove useful in the sequencing of glycans.

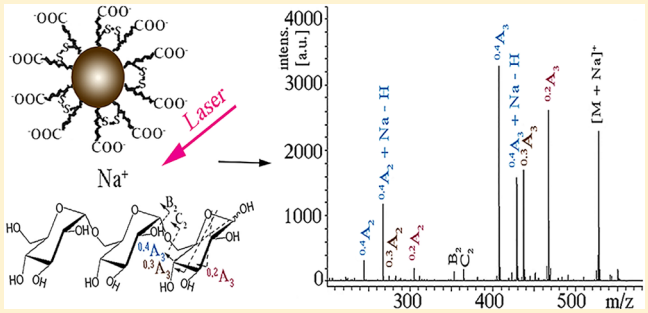

Glycans and glycoconjugates with proteins and lipids are involved in numerous biological processes such as energy storage, cell−cell communication, and membrane transport. These biomolecules play important roles in human diseases,[1,2] including muscular dystrophy, diabetes, neurodegenerative diseases, and cancer.[3−5] Identifying the specific structures of glycans is important to the understanding of their interactions with biological systems.[6] Glycan structures have been widely analyzed by mass spectrometry,[7−9] which generally provides two types of identified product ions: glycosidic and cross-ring. Glycosidic cleavages rupture the bonds between residues and provide both composition and sequence information; however, the cross-ring cleavages break bonds of a sugar ring, yielding linkage information.[10]

Glycosidic and cross-ring cleavages were originally observed by mass spectrometry in experiments involving fast atom bombardment (FAB), collision-induced fragmentation (CID), and infrared laser desorption (IRLD).[11−13] Later, softer ionization methods that more efficiently ionize large biomolecules, such as electrospray ionization (ESI) and matrix-assisted laser desorption ionization (MALDI), gained popularity.[14] Coupled to ESI or MALDI, a variety of dissociation techniques have been explored to study glycans, including high or low energy CID,[15−19] electron capture dissociation (ECD),[20] electron excitation dissociation (EED),[20] electron transfer dissociation (ETD),[10] electron detachment dissociation (EDD),[21,22] postsource decay (PSD),[23,24] and in-source decay (ISD).[23,25−27] These fragmentation techniques are associated with different mass analyzers such as quadrupole ion trap (QIT),[10,17,18] Fourier transform-ion cyclotron resonance (FT-ICR),[19−22,26] orbitrap,[19] and time-of-flight (TOF).[15,16,23,25,27] The various dissociation methods have provided complementary information and expanded glycan structural studies over different instrument platforms.

The tandem MS dissociation technique and the precursor ion identity both affect fragmentation efficiency. Glycan precursor ions in the positive mode are most commonly protonated or sodiated, although other alkaline, alkaline earth, and transition metals have also been employed as cationizing agents.[14] In the negative mode, deprotonated or chloride-adducted glycan ions have been reported.[21−23] Multiple sodium attached ions are also observed in negative mode for a highly sulfated glycosaminoglycan.[19] Positively charged protonated and sodiated glycans produce primarily glycosyl cleavages during low energy CID and PSD, whereas the negative ion mode promotes cross-ring fragmentation for both low energy CID and PSD.[23,28,29] Multiple alkaline or dication metal attachment also enhances cross-ring fragmentation for low energy

Received: July 1, 2014
Accepted: July 30, 2014
Published: July 30, 2014

CID.[12,19,30−33] High energy CID readily produces cross-ring fragmentation for sodiated glycans.[15,16] Electron-based process such as ECD, EED, and ETD on metal cation attached glycans and EDD on deprotonated and chloride-adducted glycans also produce abundant cross-ring cleavages.[10,20−22]

In-source decay (ISD) occurs in the MALDI source region directly after the desorption/ionization event and before ion extraction into the flight tube.[34−36] The mechanism of ISD may depend on the matrix employed and is believed to follow both radical-induced (ECD- or ETD-like) and thermal-activated (CID-like) pathways.[37−39] Several studies have reported that MALDI ISD produced prominent glycan cross-ring fragmentation. Yang et al.[26] performed ISD using a Nd:YAG frequency tripled laser at 90% full power on a MALDI/FT-ICR instrument with 2,5-dihydroxybenzoic acid (DHB) as the matrix. Asakawa et al.[27] observed glycan cross-ring fragmentation with an oxidizing matrix, 5-nitrosalicylic acid (5-NSA), and they proposed a hydrogen abstraction mechanism. Negative mode glycan ISD cross-ring fragmentation was reported by Yamagaki et al. using norharman (9*H*-pyrido[3,4-*b*]indole) as the matrix.[23]

A variety of nanoparticle (NP) species (e.g., gold,[40] silver,[41] platinum,[42] cadmium sulfide,[43] silicon,[44] and iron oxide[45]) exhibit strong UV absorption and have been successfully utilized as MALDI matrices. Some authors have termed such particulate matrix-based MALDI as surface-assisted laser desorption (SALDI).[46−48] The most current NP MALDI applications have been focused on peptides and small molecules and have exhibited the advantage of a clean background in the low mass-to-charge (m/z) regions of the spectra.[40−45] NP matrices for direct glycan analysis have been reported,[49−52] but little work has focused on NP matrix enhancement of glycan MALDI ISD fragmentation. In this study, for the first time we demonstrate the use of glutathione (GSH)-capped iron oxide NPs as a MALDI matrix for glycan analysis. Enhanced cross-ring ISD fragmentation is observed using a routine nitrogen laser for MALDI.

EXPERIMENTAL SECTION

Materials. For nanoparticle synthesis, the following chemicals were purchased from Thermo Fisher Scientific (Waltham, MA, U.S.A.): iron(III) chloride (ACROS, 98% purity), sodium oleate (TCL, 95%), and oleic acid (Fisher, 95%). Trioctylphosphine oxide (90%) and 1-octadecene (90%) were purchased from Sigma-Aldrich (St. Louis, MO, U.S.A.). Glutathione (97%, reduced) was purchased from Alfa Aesar (Ward Hill, MA, U.S.A.).

Chemicals for glycan analysis by mass spectrometry include glucose, sucrose, isomaltotriose, and maltoheptaose were purchased from Sigma-Aldrich. β-Cyclodextrin was purchased from VWR International (Radnor, PA, U.S.A.). Lacto-*N*-difucohexaose I (LNDFHI) and Cambridge Isotope Laboratories $H_2{}^{18}O$ (97%) were obtained from Thermo Fisher Scientific. Maltoheptaose tricosaacetate was purchased from Carbosynth US LLC (San Diego, CA, U.S.A.). The MALDI matrix 2,5-dihydroxybenzoic acid was obtained from Bruker Daltonics (Billerica, MA, U.S.A.). All the other reagents, solvents, and salts were obtained from VWR International.

Synthesis of Iron Oxide NPs. Iron oxide NPs were synthesized using a modified "heat-up" method.[53,54] In brief, iron oleate complex (the reaction precursor) was first prepared by reacting iron(III) chloride with sodium oleate in a solvent mixture (hexane/ethanol/deionized water) at 65 °C for 4 h. Then, the iron oxide nanoparticles were synthesized by heating the precursor in 1-octadecene to 315 °C in the presence of the oleic acid and trioctylphosphine oxide as the initial capping molecules. After synthesis, the nanoparticles were transferred to water through a ligand exchange method using GSH as the capping molecule.[53,54] The nanoparticles were further washed three times with distilled water through precipitation and redispersion cycles. The NP precipitation was facilitated by applying a magnet, which attracts their iron oxide core. To enhance charge repulsion and prevent NP aggregation in water, sodium hydroxide was added at a final concentration of 20 mM. The morphology and size of the iron oxide NPs were studied using a Hitachi (Tokyo, Japan) 7860 transmission electron microscope (TEM). The surface charges of the nanoparticles were measured using a Malvern (Malvern, UK) Zetasizer Nano series dynamic light scattering device. The UV−vis spectrum was collected on a Shimadzu (Kyoto, Japan) UV−vis spectrophotometer (UV-1700 series).

Glycan ^{18}O Labeling. ^{18}O labeling on the reducing end was conducted for maltoheptaose, isomaltotriose, and LNDFHI.[10] 2-Aminopyridine (2.7 mg) was added to 1 mL of anhydrous methanol to make the catalyst solution, and subsequently, 1.5 μL of catalyst solution, 20 μL of $H_2{}^{18}O$ (97%), and 0.8 μL of acetic acid were added to 1 μg of dry native glycans. The mixture was incubated at 40 °C for 16 h and then used directly for MALDI analysis.

Mass Spectrometry. MALDI ISD experiments were performed using a Bruker Daltonics Ultraflex MALDI/TOF mass spectrometer with linear and reflectron modes and a total flight tube distance of 3.2 m. An LTB Lasertechnik Berlin (Berlin, Germany) MNL100 nitrogen laser with 337 nm wavelength pulsed at 150 μJ/3 ns was used to ionize and excite the samples. All glycan samples were prepared at 0.1 mg/mL in water, and mixed with the nanoparticle matrix (0.1 mg/mL) at a 1:1 ratio. One microliter of the analyte/matrix solution was then applied to a Bruker AnchorChip target.[55,56] The hydrophilic inner surface of the AnchorChip attracted and concentrated the analyte and matrix, whereas the AnchorChip's hydrophobic outer surface kept the mixture droplet from spreading. To remove impurities remaining in the NP matrices, 2 μL of 67:33 (v/v) chloroform/methanol was applied to the dried sample spot and removed quickly with a pipet tip. For comparison experiments, DHB matrix was prepared at a concentration of 5 mg/mL in 50:50 acetonitrile/water with 0.1% trifluoroacetic acid. The mass spectra were acquired in reflectron and linear modes, with signal averaging of 200 scans. Normally, 65−75% of the maximum laser power was employed.

Electrospray ionization (ESI) experiments were performed on a Bruker HCTultra PTM Discovery System high-capacity quadrupole ion trap mass spectrometer. Glycan sample (0.1 mg/mL, 50/50 acetonitrile/water) was infused into the ESI source with a syringe pump at a rate of 200 μL/h. Nitrogen heated to 300 °C was used as the nebulizing gas with a pressure of 10 psi and the drying gas at 5 L/min. Mass spectra were collected in positive mode using a capillary voltage of approximately −3500 V with the ESI needle held at ground.

RESULTS AND DISCUSSION

Synthesis of GSH-Capped NP Matrix. The nanoparticles were synthesized using our modified heat-up method,[53,54,57−60] which produces iron oxide nanoparticles with a controlled narrow size distribution and selective surface coatings.[53] The particles used here are spherical with a diameter of 12 nm and a

dx.doi.org/10.1021/ac502422a | *Anal. Chem.* 2014, 86, 8496−8503

size variation of less than 10%. The nanoparticle dimension is limited by the synthesis technique to 4−25 nm. Above 25 nm, the magnetic interaction between the particles readily causes aggregation during the magnetic field-assisted particle precipitation, whereas smaller nanoparticles (<4 nm) have such high surface area that the surface functionalization and purification become difficult. Unlike metallic nanoparticles (e.g., Au or Ag), the optical absorbance of iron oxide nanoparticles is not sensitive to particle size and shape (Supplemental Figure S-1), which is useful for MALDI matrix application. The surface coatings directly affect the matrix interaction with the analytes, which defines the type of samples to be analyzed.

After synthesis, the iron oxide nanoparticles are only soluble in nonpolar organic solvents. A ligand exchange method was recently developed to attach desired water-soluble molecules onto the iron oxide nanoparticle surfaces.[53] The success of this approach is based on the design of introducing a ligand with a low affinity to iron oxide nanoparticle, trioctylphosphine oxide (TOPO), as a cocapping molecule during synthesis. The introduction of TOPO molecules is critical for the surface functionalization. The reason for this is that the weaker binding affinity of TOPO molecules to iron oxide surfaces and their bulky C8 tails create preferred sites or "naked" spots on the nanoparticle surfaces for hydrophilic ligands to attach or bond,[61,62] ensuring an effective ligand exchange process. In the present study, GSH functions as the surface-capping molecule, with its amino group, $—NH_2$, attached to the nanoparticle surface via Fe−N coordination, leaving its carboxylic acid group, —COOH, facing outward. Disulfide bond formation between the capping molecules further stabilizes the capping layer, and the surface carboxylic groups create a negatively charged surface, whose structure is shown in Figure 1a. The negatively charged surfaces of the nanoparticles are further confirmed by their zeta-potential measurement of −50 mV, as shown in Figure 1b.

Zeta-potential is an electrokinetic potential describing the surface potential between particle electric double layer and the surrounding medium.[63] The zeta-potential value is a stability indicator of a NP dispersion, where a colloidal system is generally stable if its zeta potential is higher than 30 mV or smaller than −30 mV.[64] For the iron oxide NPs, their high absolute value (50 mV) of the zeta potential indicates high stability of the NP water dispersion. The negative zeta-potential of the GSH-coated NPs further supports the hypothesis that the amino groups of GSH are attached to the NP surfaces, leaving the carboxylic groups oriented outward, which enhances water solubility. In addition, sodium hydroxide (20 mM) was added to prevent aggregation of the charged nanoparticles. The TEM image of Figure 1c demonstrates that the GSH-capped (12 nm diameter) nanoparticles are highly uniform, well-dispersed, and free of aggregation. Figure 1d shows the UV−vis absorption spectrum of the 12 nm GSH-capped iron oxide nanoparticles. The nanoparticles exhibit a strong absorption below 400 nm, which is within the optimal range of the MALDI laser (337 nm) used in the mass spectrometry experiments and should facilitate energy transfer from laser photons to analyte molecules.

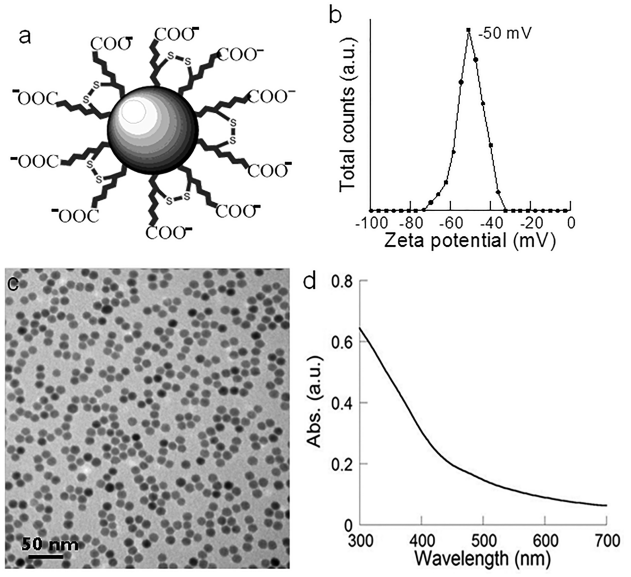

Figure 1. Characterization of GSH-capped NP: (a) schematic drawing of the structure, (b) zeta-potential plot of the NP dispersion, (c) TEM image of the NP size distribution, and (d) UV−vis absorption spectrum of the NP dispersion.

MALDI Ionization of Glycans with a GSH-Capped NP Matrix. GSH-capped NPs demonstrate unique properties for glycan analysis by MALDI. Compared to the traditional organic matrix DHB, GSH-capped NPs provide a much cleaner mass spectral background in the region below m/z 500, while maintaining a strong analyte ion signal and good signal-to-noise ratio. As shown in Figure 2a, using a GSH-capped NP matrix,

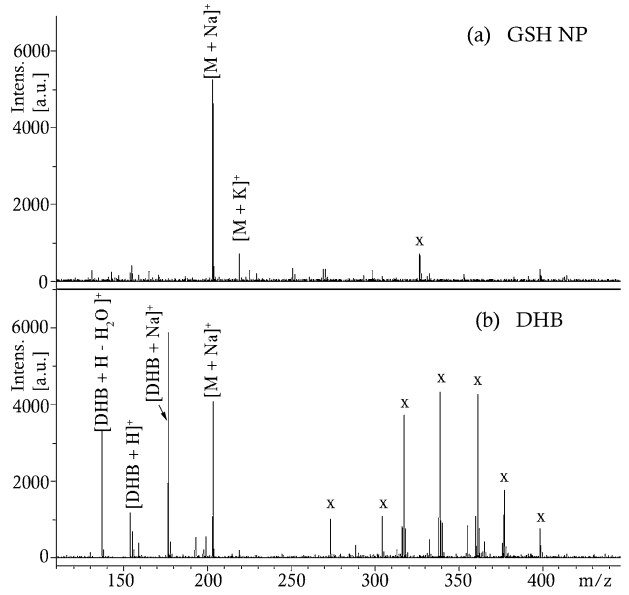

Figure 2. MALDI/TOF mass spectra of glucose (0.1 mg/mL in water) acquired using (a) GSH-capped NP matrix and (b) DHB. Peaks marked with x are ions from the matrix.

the mass spectrum of glucose is dominated by $[M + Na]^+$ with minimal background ions from the matrix. In contrast, using the conventional matrix DHB as shown in Figure 2b, matrix peaks are prominent and result in a noisy spectral background. The clean background and the intense signal using the GSH-capped NP matrix is believed to result from several factors. First, nanoparticles are heavy and are surface-bound during analyte desorption, which should greatly minimize their ability to ionize during the MALDI process. Second, the matrix is very clean because any small molecule impurities during synthesis

dx.doi.org/10.1021/ac502422a | Anal. Chem. 2014, 86, 8496−8503

are easily removed by concentrating nanoparticles with a magnet and then washing with solvents. In addition, on-target washing during sample preparation further removes impurities. (For instance, a chloroform/methanol on-target wash effectively removes lipids contaminant originating from the synthesis.) Third, the strong glycan ion signal intensity of Figure 2a suggests that efficient sample-matrix mixing and energy transfer are achieved. Ion intensity may be enhanced because the sodium counterions that are present in the electric double layer of the negatively charged NP surface readily serve as the ionization cationizing agents for $[M + Na]^+$.

The NP−Na^+−glycan interaction and energy transfer is sufficiently efficient to cause abundant cross-ring ISD fragmentation for glycans with a sugar chain length greater than two, as discussed below. In contrast, the monomer glucose does not show significant ISD fragmentation, while the ISD spectrum of sucrose (with two sugar units) only shows glycosidic cleavage products. Several glycans containing three to seven sugar units were utilized as model compounds to evaluate the MALDI ISD effectiveness of the GSH-capped NP matrix. The product ions discussed below are assigned using Domon and Costello nomenclature.[11]

ISD of Maltoheptaose and Isomaltotriose. Isomaltotriose and maltoheptaose are linear α-D-glucosyl sugars, with three and seven sugar units, respectively, and different linkage types (1 → 6 versus 1 → 4). Figures 3 and 4 show their

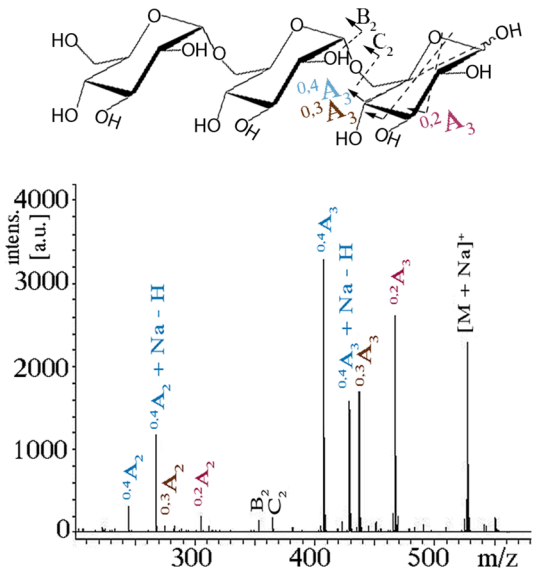

Figure 3. MALDI/TOF ISD mass spectrum of isomaltotriose acquired using a GSH-capped NP matrix. All cleavage products retain one Na^+ from the precursor $[M + Na]^+$ except $[^{0,4}A_n + Na - H]^+$, which has attachment of two Na^+.

MALDI ISD spectra. For both compounds $[M + Na]^+$ is the primary precursor ion, and cross-ring cleavages are more intense than glycosidic cleavages (B_n, C_n/Y_n). In the maltoheptaose spectra, the $[M + K]^+$ precursor ion and related fragmentation are also observed, albeit of lower intensity. $^{2,4}A_n$ and $^{0,2}A_n$ and corresponding water loss ions are generated from the 1 → 4 linked maltoheptaose. $^{0,4}A_n$, $^{0,3}A_n$, and $^{0,2}A_n$ occur from the 1 → 6 linked isomaltotriose without further water loss. This suggests the possibility of differentiating linkages based on fragmentation pattern using the GSH-capped NP induced ISD. If not specified, all cleavage products in Figures 3 and 4 retain one Na^+ or K^+ from the precursor ions. For $^{2,4}A_n$ or $^{0,4}A_n$, ion series with an extra Na replacing a H, $[^{2,4}A_n + Na - H]^+$ and $[^{0,4}A_n + Na - H]^+$, are also observed. These ions may be formed from disodium adducted precursor ions, $[M + 2Na - H]^+$; the absence of such precursor ions in the spectra indicates that these disodiated ions are more readily dissociated. The fact that only $^{2,4}A_n$ or $^{0,4}A_n$ disodium ions are observed may suggest these glycan fragments better stabilize the two adducted sodium ions. This is consistent with the observation that dilithiated carbohydrates produce primarily $^{2,4}A_n$ or $^{0,4}A_n$ as CID product ions for 1 → 4, and 1 → 6 linkages, respectively.[12]

Because the reducing end and nonreducing end product ions for maltoheptaose and isomaltotriose are degenerate in mass, ^{18}O labeling of the anomeric carbon was performed to clarify assignment ambiguity. After ^{18}O labeling, product ions from the reducing end (Y, Z, and X) experience a mass shift of 2 Da, whereas the masses of product ions from the nonreducing end (B, C, and A) are unchanged. Both maltoheptaose and isomaltotriose ^{18}O labeling produced only very slight ion intensity growth for peaks 2 Da higher than the ambiguous C_n/Y_n product ions, indicating that the majority of the observed glycosidic and cross-ring product ions originate from the nonreducing end (B, C, and A). Thus, ambiguous C_n/Y_n ions are labeled as C_n in the mass spectra.

ISD of Lacto-*N*-difucohexaose I (LNDFHI). Figure 5 shows the ISD spectrum of a branched glycan, lacto-*N*-difucohexaose, LNDFHI. The C-ion series is complete and intense, whereas the B- and Y-ion series are incomplete and weak. No Z-ions are present. The branch point GlcNAc shows no cross-ring fragmentation, and multiple glycosidic bonds cleave simultaneously. Fucose loss readily occurs, either directly from $[M + Na]^+$ ($Y_{4\alpha}/Y_{3\beta}$) or from product ions ($B_3 - F$, $C_3 - F$, $^{2,4}A_4 - F$, $^{1,4}A_4 - F$, $B_3 - 2F$). In one case, the complete α chain is lost from a B3 fragment ($Y_{3\alpha}B_3$). The product ions $B_3 - F$, $C_3 - F$, $^{2,4}A_4 - F$, $^{1,4}A_4 - F$ could also be assigned as complete α chain loss from B_4, C_4, $^{2,4}A_5$, and $^{1,4}A_5$ ions.

^{18}O labeling of the anomeric carbon helped to clarify ambiguous assignments. For example, m/z 816.1 could be $^{1,3}X_{3\alpha}$ or $^{0,2}A_5 - F$. In the ^{18}O-labeled spectra, this mass does not show distinctive intensity growth for $[M + 2]$ (m/z 818.1), thus the ion is assigned to $^{0,2}A_5 - F$. Similarly, m/z 714.1 is assigned to $C_4 - F$ rather than $Y_{3\alpha}$. In the ^{18}O labeled spectrum, a product ion that undergoes an increase in $[M + 2]$ intensity is $Y_{4\alpha}/Y_{3\beta}$ (m/z 876). The ^{18}O labeling results indicate that there are no distinctive X cleavages by ISD and that A cleavages dominate the cross-ring fragmentation.

ISD of β-Cyclodextrin. Figure 6 shows the ISD spectrum of the cyclic glycan β-cyclodextrin. Multiple sodium attachment $[M + nNa - (n - 1)H]^+$, n = 1−3, is more prominent than in the spectra of the linear and branched glycans. This is likely because the cyclodextrin cavity readily allows coordination of alkaline metal ions. For example, multiple lithium attachment during ESI has been reported by Madhusudanan.[30] Even though two bonds must cleave before product ions can be observed for a cyclic glycan, abundant fragmentation is found in the ISD spectrum of sodiated β-cyclodextrin. There is a series of ions resulting from consecutive sugar unit loss (m/z 185, 347, 509, 671, 833, 995) by double glycosidic bond cleavages. There also is an ion series formed by a $^{2,4}A$ cleavage, as well as glycosidic Z cleavages (m/z 227, 389, 551, 713, 875, and 1037). Because these ions contain one Na^+, the consecutive sugar unit loss and $^{2,4}A + Z$ fragmentation are most likely produced from $[M + Na]^+$ precursor ions. In addition, several ion series are

dx.doi.org/10.1021/ac502422a | Anal. Chem. 2014, 86, 8496−8503

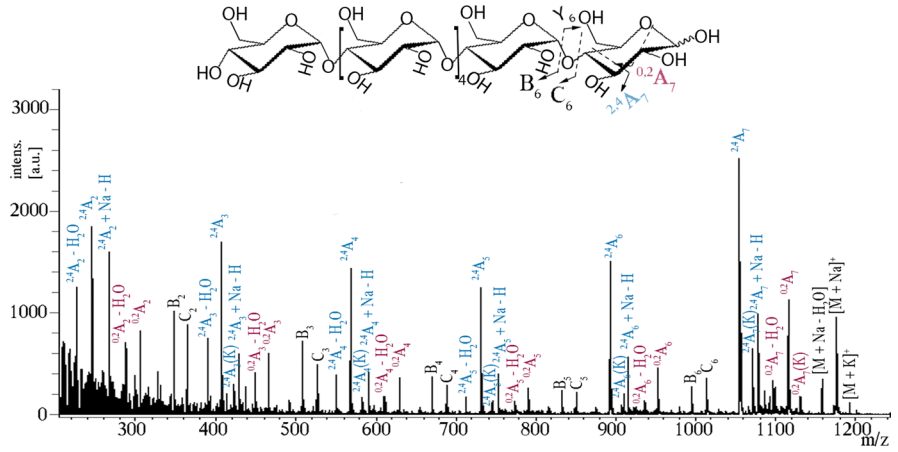

Figure 4. MALDI/TOF ISD mass spectrum of maltoheptaose acquired using a GSH-capped NP matrix. If not specified, all cleavage products retain one Na^+ from the precursor ion $[M + Na]^+$. Product ions generated from $[M + K]^+$ are labeled as $A_n(K)$, although $[^{2,4}A_n + Na - H]^+$ have two Na^+ attached.

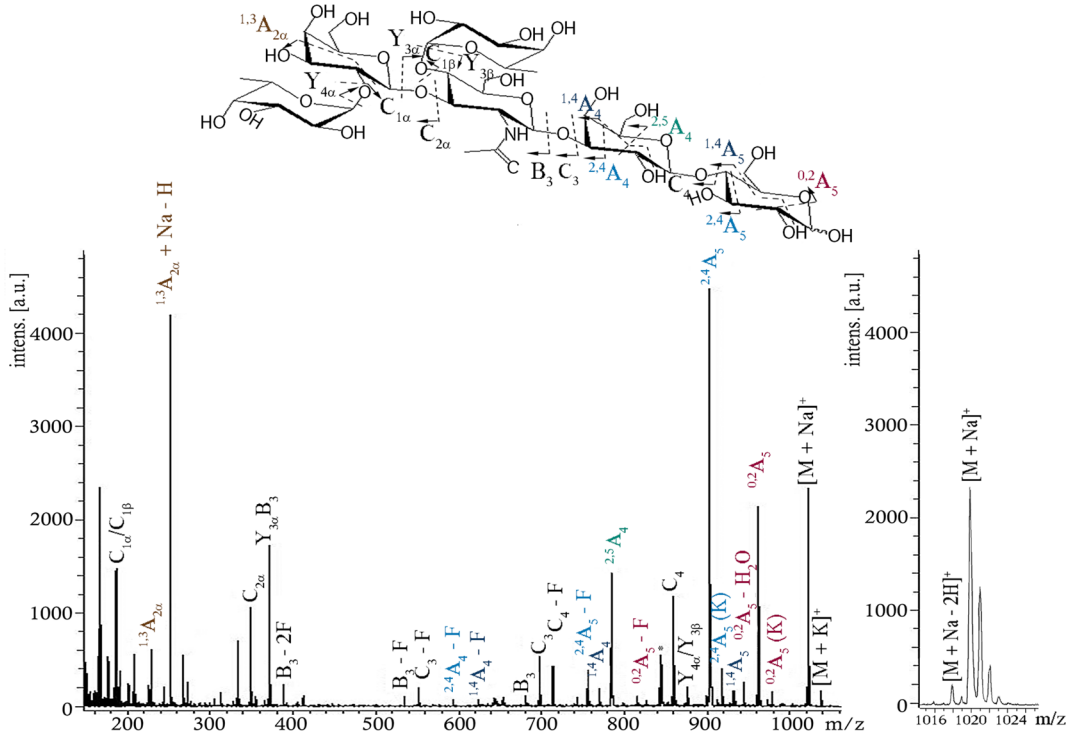

Figure 5. MALDI/TOF ISD mass spectrum of lacto-*N*-difucohexaose I (LNDFHI) acquired using a GSH-capped NP matrix. Fucose sugar unit loss (−F) from $[M + Na]^+$ ($Y_{4\alpha}/Y_{3\beta}$) or from product ions ($B_3 - F$, $C_3 - F$, $^{2,4}A_4 - F$, $^{1,4}A_4 - F$, $B_3 - 2F$) is observed. * indicates peaks with poor resolution, likely metastable ions. The expansion shows the presence of $[M + Na - 2H]^+$ in the precursor ion region.

formed by a $^{2,4}A$ cleavage, as well as glycosidic Y cleavages with one, two, or three Na^+ (m/z 245, 407, 569, 731, 893; 267, 429, 591, 753, 915; 289, 451, 613, 775, 937, respectively). These ions are likely produced from single or multiple Na^+ attached precursor ions. Overall, ion series formed by combined cross-ring and glycosidic cleavages ($^{2,4}A + Y$ and $^{2,4}A + Z$) are more intense than the double glycosidic cleaved (consecutive sugar unit loss) ion series.

Several cyclodextrin dissociation studies have reported consecutive sugar unit loss with or without cross-ring and glycosidic combined cleavages.[26,28,30,31] Cross-ring and glycosidic combined cleavages were observed by negative PSD for $[M - H]^+$ precursors and by low energy CID for multiple lithium or doubly charged metal ion attached precursors.[28,30,31] In comparison, ISD spectra taken with a Nd:YAG frequency tripled laser at 90% full power in a Fourier transform ion cyclotron resonance (FT-ICR) mass spectrometer using DHB as matrix only yielded product ions from consecutive sugar units loss.[26] Here, we demonstrate that combined cross-ring and glycosidic cleavages ($^{2,4}A + Y$ and $^{2,4}A + Z$) are also observed in MALDI ISD for $[M + nNa - (n - 1)H]^+$, $n = 1–3$, precursors using a GSH-capped NP matrix. This observation further demonstrates that the iron oxide NP matrix allows facile energy transfer to the analyte.

Mechanism of ISD on Glycans. Asakawa and co-workers have reported that 5-nitrosalicylic acid (5-NSA) matrix induces native glycan cross-ring fragmentation through hydrogen abstraction from the hydroxyl groups of glycans, −OH.[27]

dx.doi.org/10.1021/ac502422a | *Anal. Chem.* 2014, 86, 8496−8503

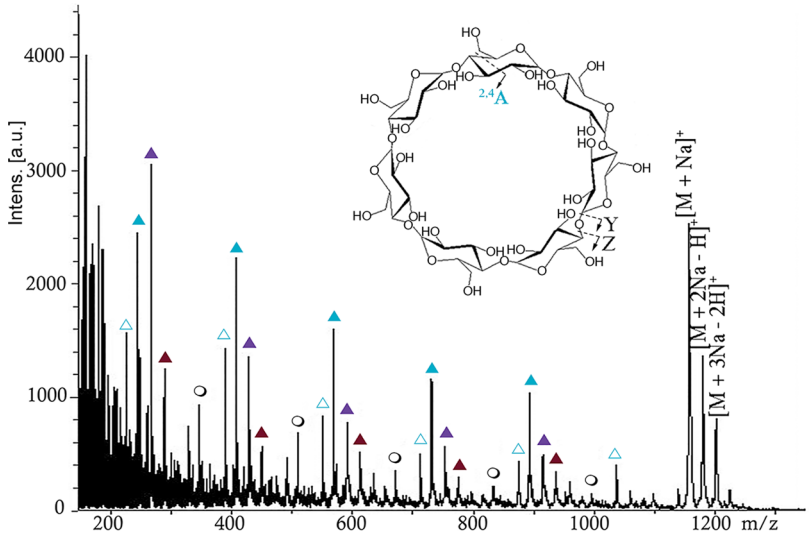

Figure 6. MALDI/TOF ISD mass spectrum of β-cyclodextrin acquired using a GSH-capped NP matrix. The fragmentation shows consecutive sugar unit loss by glycosidic bond cleavages (◯) and ^{2,4}A + Z (blue outline △) or ^{2,4}A + Y (solid blue ▲) type cleavages from the $[M + Na]^+$ precursor ions. ^{2,4}A + Y type cleavages also show disodium (purple ▲) or trisodium (magenta ▲) attached series. Multiple sodium attachment for the precursor ions is prominent.

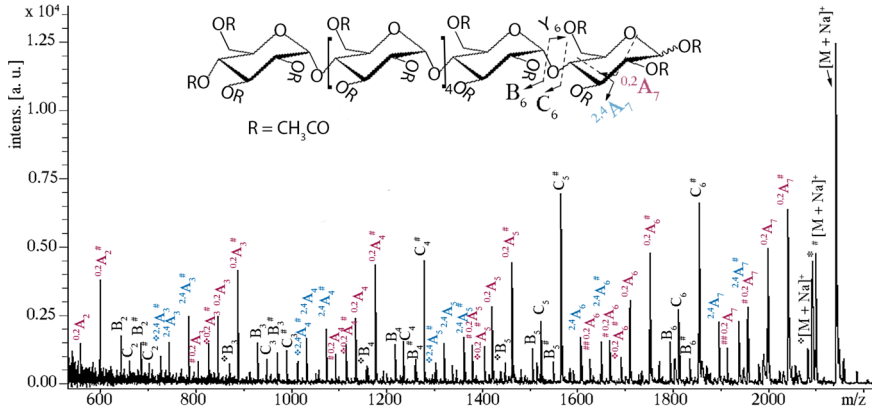

Figure 7. MALDI/TOF ISD mass spectrum of maltoheptaose tricosaacetate acquired using a GSH-capped NP matrix. R = CH_3CO. * indicates peaks with poor resolution, likely metastable ions. Abundant loss of 42 Da (CH_2CO) and 60 Da (CH_3COOH) are observed from both precursor and product ions. # to the left side of a symbol means extra loss of 42, whereas ## to the left side means extra loss of 2 × 42. # to the right side of a symbol means extra gain of 42 Da. Loss of 60 is denoted by a box diamond symbol to the left side of a symbol. For instance, ◆$^{2,4}A_5^{\#}$ means a direct $^{2,4}A_5$ cleavage gained extra CH_2CO through rearrangement and had a neutral loss of CH_3COOH.

These researchers proposed that the presence of a hydrogen-deficient glycan radical, $[M - H]^{\bullet}$, led to enhanced ISD fragmentation. This hydrogen abstraction mechanism was based on their observation that for native glycans $[M + Na]^+$ precursor and ISD product ions, as well as the oxidized precursor, $[M - 2H + Na]^+$ were present. For permethylated glycans where −OH is replaced by a methoxy group, $-OCH_3$, both the oxidized precursor and ISD fragmentation were absent, with $[M + Na]^+$ as the base peak.[27]

With the GSH-capped NP matrix, $[M - 2H + Na]^+$ is also observed for maltoheptaose, isomaltotriose, and LNDFHI at 3%, 12%, and 19% in peak height compared to the $[M + Na]^+$ intensity, respectively. Figure 5 expansion shows the presence of $[M - 2H + Na]^+$ for LNDFHI. To determine if the ISD mechanism involves hydrogen abstraction from glycan−OH groups, MALDI ISD spectra using GSH-capped NP matrix were obtained for peracetylated maltoheptaose (maltoheptaose tricosaacetate). Even with the peracetylation modification, the ISD spectrum shows abundant cross-ring ISD product ions (Figure 7). This indicates that −OH groups are not necessary for glycan ISD fragmentation to proceed when using the GSH-capped NP matrix.

Major ion series observed in the maltoheptaose tricossacetate ISD spectrum with GSH-capped NP matrix are B_n, C_n, $^{0,2}A_n$, and $^{2,4}A_n$. Loss of 42 and 60 Da from precursor and product ions (B_n, C_n, $^{0,2}A_n$, and $^{2,4}A_n$) are observed. The 42 Da elimination is likely CH_2CO. Multiple losses of CH_2CO have been reported for peracetylated 1-phenylflavazole or arylglycosylamine sugar derivatives in electron impact ionization spectra.[65−67] Losses of 42 Da from product ions could also be due to internal cleavages (losses from two terminal sites).[68] Gain of 42 Da is also observed for product ions (B_n, C_n, $^{0,2}A_n$, and $^{2,4}A_n$) and may be the result of rearrangement involving a nearby acetyl group prior to cleavage of the backbone. The prominent 42 Da loss from the precursor ion in the ISD spectra (43% of the precursor ion) is not a contamination peak due to incomplete acetylation; it is instead an ISD product ion, because the 42 loss peak is minimal (<5% of the precursor ion)

dx.doi.org/10.1021/ac502422a | Anal. Chem. 2014, 86, 8496−8503

in an ESI MS spectrum (Supplemental Figure S-2). The 60 Da loss is undoubtedly acetic acid, CH_3COOH. The elimination of 60 Da from a C_n fragment is identical in mass to a gain of 42 Da from $^{0,2}A_n$. However, this peak series is labeled as a gain of 42 Da from $^{0,2}A_n$, because they are much more intense than the C_n series. In comparison, the $[B_n - 60]$ series is weaker than the B_n series.

The photoelectric process of iron oxide NPs upon laser irradiation is complicated. Upon photon absorption, electrons in the occupied valence band of iron oxide can be elevated to the unoccupied conduction band, leading to excited state conduction electrons and positive valence band holes. These charge carriers can recombine, dissipating heat to surface adsorbents, or participate in redox reaction with surface adsorbents.[47,69] Rapid heating upon laser radiation on nanoparticle surface drives electrons toward the cooler bulk layer and leaves positive holes on the top layer. The resulting high electric field may also transfer energy to the adsorbents in a process similar to field ionization.[47] The presence of $[M + Na - 2H]^+$ peaks in native glycans confirms the oxidation process by iron oxide. However, redox is not the only process involved, as a peracetylated glycan also demonstrates intense ISD. Combined field and thermal effects also play roles in ISD.

Other negatively charged capping molecules, such as poly(acrylic acid) or dopamine also induce efficient ISD (Supplemental Figure S-3). GSH is chosen as the matrix for this study because it provides a variety of product ions at comparable intensity. Positively charged polyethylenimine (PEI, 1 mM of HCl) capping does not cause cross-ring ISD in Figure S-3, which is likely related to the additive, HCl instead of NaOH. Na^+ ion abundance on the nanoparticle surface seems critical for glycan ISD. Na^+ ions could function as a salt bridge between the nanoparticle capping molecules and glycans, facilitating glycan particle surface adherence and thus efficient energy or charge transfer. In the meantime, Na^+ glycan attachment promotes cross-ring fragmentation. In-depth investigation on capping molecule and additive effects will be conducted in future work.

CONCLUSIONS

A GSH-capped iron oxide NP matrix is demonstrated to be effective for the analysis of glycans by MALDI mass spectrometry. Important characteristics of this new matrix include a clean mass spectral background in the low m/z region and abundant ISD fragmentation. Glycosidic and cross-ring cleavages occur for three to seven sugar unit linear, branched, and cyclic unmodified glycans. ^{18}O labeling experiments were used to clarify assignment ambiguities and showed that the majority of the fragmentation originated from the nonreducing end of the glycans. Extensive series of ISD product ions were formed in high intensity, suggesting that the GSH-capped NP matrix both absorbs strongly at the laser wavelength and has the ability to promote strong energy transfer to the analytes. The use of iron oxide NP matrices to promote fragmentation by ISD has great promise for the structural analysis of glycans and other biomolecules.

ASSOCIATED CONTENT

Supporting Information

Additional results as noted in the text. This material is available free of charge via the Internet at http://pubs.acs.org/.

AUTHOR INFORMATION

Corresponding Author

*E-mail: liang005@ua.edu.

Author Contributions

The manuscript was written through contributions of all authors.

Notes

The authors declare no competing financial interest.

ACKNOWLEDGMENTS

The authors gratefully acknowledge financial support from National Science Foundation DMR-0907204 and DMR-1149931 grants, and from a College Academy of Research, Scholarship and Creative Activity (CARSCA) grant administered through the University of Alabama's College of Arts and Sciences. Y.B. also thanks the University of Alabama Department of Biological Sciences for the use of transmission electron microscopy.

REFERENCES

(1) Hart, G. W.; Copeland, R. J. *Cell* **2010**, *143*, 672−676.
(2) Zaia, J. *Chem. Biol.* **2008**, *15*, 881−892.
(3) Yoshida-Moriguchi, T.; Yu, L.; Stalnaker, S. H.; Davis, S.; Kunz, S.; Madson, M.; Oldstone, M. B.; Schachter, H.; Wells, L.; Campbell, K. P. *Science* **2010**, *327*, 88−92.
(4) Hart, G. W.; Housley, M. P.; Slawson, C. *Nature* **2007**, *446*, 1017−1022.
(5) Zeidan, Q.; Hart, G. W. J. *Cell Sci.* **2010**, *123*, 13−22.
(6) Raman, R.; Raguram, S.; Venkataraman, G.; Paulson, J. C.; Sasisekharan, R. *Nat. Methods* **2005**, *2*, 817−824.
(7) Harvey, D. *J. Mass Spectrom. Rev.* **1999**, *18*, 349−450.
(8) North, S. J.; Hitchen, P. G.; Haslam, S. M.; Dell, A. *Curr. Opin. Struct. Biol.* **2009**, *19*, 498−506.
(9) Leymarie, N.; Zaia, J. *Anal. Chem.* **2012**, *84*, 3040−3048.
(10) Han, L.; Costello, C. E. *J. Am. Soc. Mass Spectrom.* **2011**, *22*, 997−1013.
(11) Domon, B.; Costello, C. E. *Glycoconj. J.* **1988**, *5*, 397−409.
(12) Zhou, Z.; Ogden, S.; Leary, J. A. *J. Org. Chem.* **1990**, *55*, 5444−5446.
(13) Spengler, B.; Dolce, J. W.; Cotter, R. J. *Anal. Chem.* **1990**, *62*, 1731−1737.
(14) Zaia, J. *Mass Spectrom. Rev.* **2004**, *23*, 161−227.
(15) Mechref, Y.; Novotny, M. V.; Krishnan, C. *Anal. Chem.* **2003**, *75*, 4895−4903.
(16) Stephens, E.; Maslen, S. L.; Green, L. G.; Williams, D. H. *Anal. Chem.* **2004**, *76*, 2343−2354.
(17) Ashline, D.; Singh, S.; Hanneman, A.; Reinhold, V. *Anal. Chem.* **2005**, *77*, 6250−6262.
(18) Fukui, K.; Kameyama, A.; Mukai, Y.; Takahashi, K.; Ikeda, N.; Akiyama, Y.; Narimatsu, H. *Carbohydr. Res.* **2006**, *341*, 624−633.
(19) Kailemia, M. J.; Li, L.; Ly, M.; Linhardt, R. J.; Amster, I. J. *Anal. Chem.* **2012**, *84*, 5475−5478.
(20) Yu, X.; Huang, Y.; Lin, C.; Costello, C. E. *Anal. Chem.* **2012**, *84*, 7487−7494.
(21) Kornacki, J. R.; Adamson, J. T.; Hakansson, K. *J. Am. Soc. Mass Spectrom.* **2012**, *23*, 2031−2042.
(22) Wolff, J. J.; Amster, I. J.; Chi, L.; Linhardt, R. J. *J. Am. Soc. Mass Spectrom.* **2007**, *18*, 234−244.
(23) Yamagaki, T.; Suzuki, H.; Tachibana, K. *Anal. Chem.* **2005**, *77*, 1701−1707.
(24) Spengler, B. *J. Mass Spectrom.* **1997**, *32*, 1019−1036.
(25) Smargiasso, N.; De Pauw, E. *Anal. Chem.* **2010**, *82*, 9248−9253.
(26) Yang, H.; Yu, Y.; Song, F.; Liu, S. *J. Am. Soc. Mass Spectrom.* **2011**, *22*, 845−855.
(27) Asakawa, D.; Smargiasso, N.; De Pauw, E. *Anal. Chem.* **2012**, *84*, 7463−7468.

(28) Yamagaki, T.; Nakanishi, H. *J. Mass Spectrom. Soc. Jpn.* **2002**, *50*, 204−207.
(29) Pfenninger, A.; Karas, M.; Finke, B.; Stahl, B. *J. Am. Soc. Mass Spectrom.* **2002**, *13*, 1331−1340.
(30) Madhusudanan, K. P. *J. Mass Spectrom.* **2003**, *38*, 409−416.
(31) Frański, R.; Gierczyk, B.; Schroeder, G.; Beck, S.; Springer, A.; Linscheid, M. *Carbohydr. Res.* **2005**, *340*, 1567−1572.
(32) Fura, A.; Leary, J. A. *Anal. Chem.* **1993**, *65*, 2805−2811.
(33) Salpin, J. Y.; Tortajada, J. *J. Mass Spectrom.* **2002**, *37*, 379−388.
(34) Brown, R. S.; Lennon, J. J. *Anal. Chem.* **1995**, *67*, 3990−3999.
(35) Reiber, D. C.; Grover, T. A.; Brown, R. S. *Anal. Chem.* **1998**, *70*, 673−683.
(36) Takayama, M. *J. Am. Soc. Mass Spectrom.* **2001**, *12*, 420−427.
(37) Hardouin. *J. Mass Spectrom. Rev.* **2007**, *26*, 672−682.
(38) Demeure, K.; Gabelica, V.; De Pauw, E. A. *J. Am. Soc. Mass Spectrom.* **2010**, *21*, 1906−1917.
(39) Smargiasso, N.; Quinton, L.; De Pauw, E. *J. Am. Soc. Mass Spectrom.* **2012**, *23*, 469−474.
(40) McLean, J. A.; Stumpo, K. A.; Russell, D. H. *J. Am. Chem. Soc.* **2005**, *127*, 5304−5305.
(41) Sherrod, S. D.; Diaz, A. J.; Russell, W. K.; Cremer, P. S.; Russell, D. H. *Anal. Chem.* **2008**, *80*, 6796−6799.
(42) Shrivas, K.; Agrawal, K.; Wu, H. *Analyst* **2011**, *136*, 2852−2857.
(43) Kailasa, S. K.; Wu, H. *Rapid Commun. Mass Spectrom.* **2011**, *25*, 271−280.
(44) Wen, X.; Dagan, S.; Wysocki, V. H. *Anal. Chem.* **2007**, *79*, 434−444.
(45) Tseng, M.; Obena, R.; Lu, Y.; Lin, P.; Lin, P.; Yen, Y.; Lin, J.; Huang, L.; Lu, K.; Lai, L.; Lin, C.; Chen, Y. *J. Am. Soc. Mass Spectrom.* **2010**, *21*, 1930−1939.
(46) Sunner, J.; Dratz, E.; Chen, Y. *Anal. Chem.* **1995**, *67*, 4335−4342.
(47) Law, K. P.; Larkin, J. R. *Anal. Bioanal. Chem.* **2011**, *399*, 2597−2622.
(48) Aminlashgari, N.; Hakkarainen, M. *J. Am. Soc. Mass Spectrom.* **2012**, *23*, 1071−1076.
(49) Su, C.; Tseng, W. *Anal. Chem.* **2007**, *79*, 1626−1633.
(50) Lin, P.; Tseng, M.; Su, A.; Chen, Y.; Lin, C. *Anal. Chem.* **2007**, *79*, 3401−3408.
(51) Gholipour, Y.; Giudicessi, S. L.; Nonami, H.; Erra-Balsells, R. *Anal. Chem.* **2010**, *82*, 5518−5526.
(52) Harvey, D. *J. Mass Spectrom. Rev.* **2014**, DOI: 10.1002/mas.21411.
(53) Xu, Y.; Qin, Y.; Palchoudhury, S.; Bao, Y. *Langmuir* **2011**, *27*, 8990−8997.
(54) Xu, Y.; Palchoudhury, S.; Qin, Y.; Macher, T.; Bao, Y. *Langmuir* **2012**, *28*, 8767−8772.
(55) Schuerenberg, M.; Luebbert, C.; Eickhoff, H.; Kalkum, M.; Lehrach, H.; Nordhoff, E. *Anal. Chem.* **2000**, *72*, 3436−3442.
(56) Gobom, J.; Schuerenberg, M.; Mueller, M.; Theiss, D.; Lehrach, H.; Nordhoff, E. *Anal. Chem.* **2001**, *73*, 434−438.
(57) Palchoudhury, S.; Xu, Y.; Goodwin, J.; Bao, Y. *J. Appl. Phys.* **2011**, *109*, 07E314.
(58) Palchoudhury, S.; Xu, Y.; Goodwin, J.; Bao, Y. *J. Mater. Chem.* **2011**, *21*, 3966−3970.
(59) Palchoudhury, S.; An, W.; Xu, Y.; Qin, Y.; Zhang, Z.; Chopra, N.; Holler, R. A.; Turner, C. H.; Bao, Y. *Nano Lett.* **2011**, *11*, 1141−1146.
(60) Palchoudhury, S.; Xu, Y.; Rushdi, A.; Holler, R. A.; Bao, Y. *Chem. Commun.* **2012**, *48*, 10499−10501.
(61) Palchoudhury, S.; Xu, Y.; An, W.; Turner, C. H.; Bao, Y. *J. Appl. Phys.* **2010**, *107*, 09B311.
(62) Bao, Y.; Beerman, M.; Pakhomov, A. B.; Krishnan, K. M. J. *Phys. Chem. B* **2005**, *109*, 7220−7222.
(63) Hunter, R. J. *Zeta Potential in Colloid Science: Principles and Application*; Academic Press: London, 1981.
(64) Taboada, E.; Rodríguez, E.; Roig, A.; Oró, J.; Roch, A.; Muller, R. N. *Langmuir* **2007**, *23*, 4583−4588.
(65) Johnson, G. S.; Ruliffson, W. S.; Cooks, R. G. *Carbohydr. Res.* **1971**, *18*, 243−249.
(66) Johnson, G. S.; Ruliffson, W. S.; Cooks, R. G. *Carbohydr. Res.* **1971**, *18*, 233−242.
(67) Chizhov, O.; Malysheva, N.; Kochetkov, N. *Carbohydr. Res.* **1973**, *28*, 21−29.
(68) Harvey, D. *J. Proteomics* **2005**, *5*, 1774−1786.
(69) Beydoun, D.; Amal, R.; Low, G.; McEvoy, S. *J. Nanopart. Res.* **1999**, *1*, 439−458.